Chemical Science

EDGE ARTICLE

Galbofloxacin: a xenometal-antibiotic with potent *in vitro* and *in vivo* efficacy against *S. aureus*†

Apurva Pandey, Dariusz Śmiłowicz and Eszter Boros ⓘD *

Siderophore-antibiotic drug conjugates are considered potent tools to deliver and potentiate the antibacterial activity of antibiotics, but only few have seen preclinical and clinical success. Here, we introduce the gallium(III) complex of a ciprofloxacin-functionalized linear desferrichrome, Galbofloxacin, with a cleavable serine linker as a potent therapeutic for *S. aureus* bacterial infections. We employed characterization using *in vitro* inhibitory assays, radiochemical, tracer-based uptake and pharmacokinetic assessment of our lead compound, culminating in *in vivo* efficacy studies in a soft tissue model of infection. Galbofloxacin exhibits a minimum inhibitory concentration of (MIC_{98}) 93 nM in wt *S. aureus*, exceeding the potency of the parent antibiotic ciprofloxacin (0.9 μM). Galbofloxacin is a protease substrate that can release the antibiotic payload in the bacterial cytoplasm. Radiochemical experiments with *wt* bacterial strains reveal that ^{67}Galbofloxacin is taken up efficiently using siderophore mediated, active uptake. Biodistribution of ^{67}Galbofloxacin in a mouse model of intramuscular *S. aureus* infection revealed renal clearance and enhanced uptake in infected muscle when compared to ^{67}Ga-citrate, which showed no selectivity. A subsequent *in vivo* drug therapy study reveals efficient reduction in *S. aureus* infection burden and sustained survival with Galbofloxacin for 7 days. Ciprofloxacin had no treatment efficacy at identical molecular dose (9.3 μmol kg^{-1}) and resulted in death of all study animals in <24 hours. Taken together, the favorable bacterial growth inhibitory, pharmacokinetic and *in vivo* efficacy properties qualify Galbofloxacin as the first rationally designed Ga-coordination complex for the management of *S. aureus* bacterial infections.

Introduction

Infectious diseases are one of the leading causes of death worldwide.[1] Among infective agents, the Gram-positive pathogen *Staphylococcus aureus* (*S. aureus*) can trigger a variety of pathologies, such as skin and soft tissue infections, endocarditis, osteomyelitis, lethal pneumonia, and causes the majority of hospital acquired bacterial infections and deaths in the United States.[2,3] Depending on the susceptibility of pathogen towards currently used antibiotics, *S. aureus* can be divided into MSSA (methicillin susceptible *S. aureus*) and MRSA (methicillin resistant *S. aureus*).[4] In recent decades, the opioid epidemic and the over-prescription of antibiotics, has resulted in rapid emergence of drug resistant *S. aureus* worldwide. The incidence of infection requiring hospital care has increased, yet clinical treatment of MRSA has become more challenging. The emergence of bacteria with resistance to currently used

antibiotics, combined with the paucity of new compounds in the pipeline necessitates the development of targeted novel antibiotics with new mechanisms of action.[5,6]

Bacterial virulence is closely associated with nutrient acquisition, which is essential for bacterial growth and proliferation.[7] During an infection, iron – an indispensable micronutrient, essential for a plethora of cellular reactions in both humans and pathogens, is restricted for bacterial uptake as the available iron is tightly sequestered by host proteins such as – hemoglobin, transferrin and ferritin.[7] Bacteria rely on scavenging essential transition metal ions from their host, specifically iron in the form of ferrous/ferric (Fe^{2+}/Fe^{3+}). The low solubility of $Fe(OH)_3$ ($K_{sp} = 6.3 \times 10^{-38}$) at pH 7.4 results in an insufficient quantity of iron for bacteria to grow. Given the essential role of iron (Fe) in bacterial physiology and pathogenicity, and the ability of bacteria to actively transport essential nutrient suggests that the iron uptake and metabolism pathway can be highjacked for development of new theranostic agents that can circumvent the membrane permeability barrier of bacteria.[8] Consequently, to maintain the Fe homeostasis and counteract iron limitation, bacteria have developed iron uptake strategies, by producing low molecular weight, water soluble iron chelators called siderophores.[9]

Siderophore-antibiotic conjugates are a compound class with a long history of efficacy against various bacterial strains.

Department of Chemistry, Stony Brook University, 100 Nicolls Road, Stony Brook, New York 11790, USA. E-mail: eszter.boros@stonybrook.edu

These conjugates act as Trojan horses for delivery of antibiotics across the bacterial membrane, taking advantage of the Fe assimilation pathway in bacteria.[10–16] In 2019, the FDA (Food and Drug Administration) approved cefiderocol (Fig. 2), a siderophore based antibiotic conjugate for treatment of complicated urinary tract infections (cUTI).[17] The conjugate consists of a bidentate catechol siderophore moiety that promotes the formation of chelated complexes with ferric iron and thereby facilitates siderophore-like transport across the outer bacterial membrane and a beta lactam-based cephalosporin drug counterpart.[18] The conjugate is active against carbapenem-resistant Enterobacteriaceae (CRE) and extended-spectrum beta-lactamases (ESBLs) producing bacteria.[19,20] However, the bidentate coordinating donor site limits recognition by a large fraction of Fe-siderophore transport proteins, especially those accessing the cytoplasm.[21,22]

While the coordinating moiety is not essential for periplasm targeting antibiotics such as cefiderocol, it could significantly limit siderophore-mediated delivery of antibiotics that interact with a cytoplasmic target. In this regard, a more complete, tetra- or even hexacoordinate, siderophore-like motifs are desired, as they are more efficiently recognized and able to be transported to the cytoplasm (Fig. 1). However, the successful demonstration of *in vivo* potency of other hexadentate siderophore antibiotic conjugates remains scarce.[23,24] Two primary reasons emerge as the possible cause for this significant knowledge and data gap: (1) a common hypothesis for the lack of translatability of these constructs due to their need for an iron depleted environment for efficacy and (2) a sensitivity to premature proteolytic degradation of hexadentate siderophores in mammalian plasma.

Previously, we introduced the Ga^{3+} complex of the hexadentate, ornithine-derived tripeptide siderophore linear desferrichrome (LDFC) linked to the FDA approved antibiotic, ciprofloxacin *via* a beta-alanine linker, Ga-**D2**.[25] We showed that the complexation with the xenometal Ga(III) produces enhanced potency when compared with the apo-(metal free) or endogenous metal ion (Fe)-bound siderophore conjugate.[25] Our work was inspired by the structure of the natural product and antibiotic albomycin (Fig. 2) and the recent clinical success of $Ga(NO_3)_3$ (ref. 26–29) in a phase 1 trial for treatment of *Pseudomonas aeruginosa* (*P. aeruginosa*) lung infections in adults with cystic fibrosis (CF).[28] $Ga(NO_3)_3$ imparted significant therapeutic effects.[30] However, the drug was dosed at a high concentration of 200 mg per m^2 per day for 5 days, so we posited that delivery of the Ga cargo with a siderophore-conjugate could significantly reduce dosing needs. Indeed, our first-generation construct Ga-**D2** (Fig. 2) demonstrated good, broad spectrum potency in *E. coli*, *S. aureus*, *P. aeruginosa* and *Klebsiella pneumoniae* (*K. pneumoniae*) with a minimum inhibitory
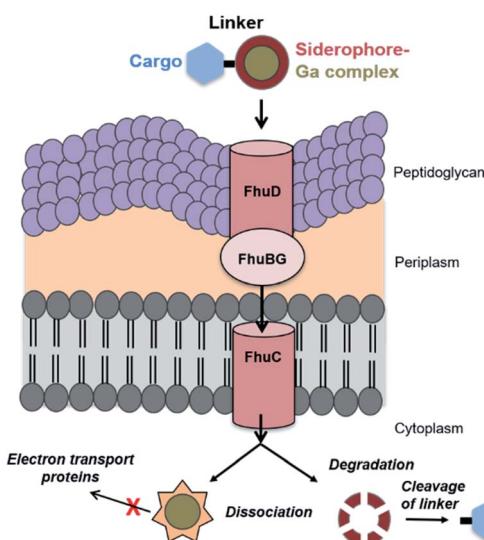
Fig. 1 Proposed transport internalization pathway for ferrichrome based Galbofloxacin in wt *S. aureus* using active transmembrane transport.
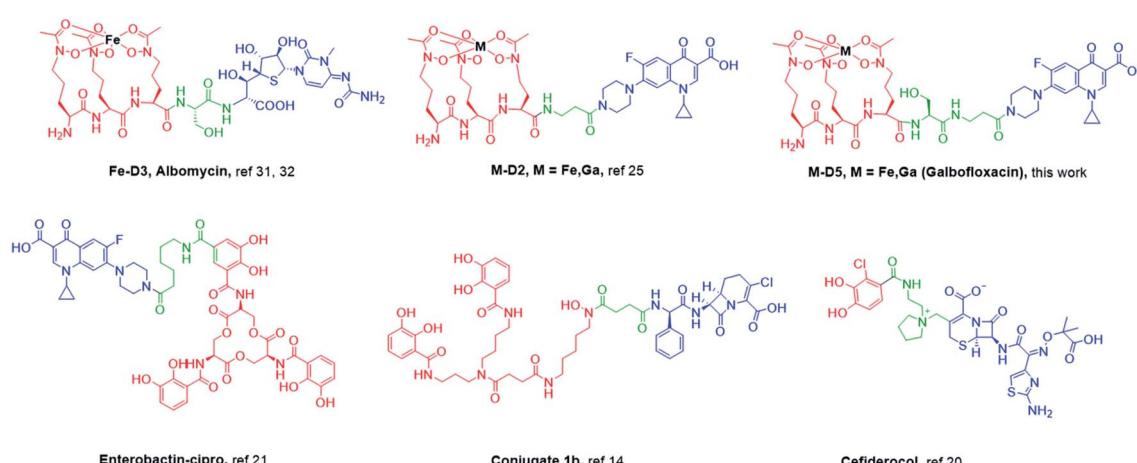
Fig. 2 Chemical structures of (top panel) structurally related hydroxamate siderophore–antibiotic conjugates synthesized and investigated previously, as well as subject of studies in this work: **D2**, **D5**, albomycin (Fe-**D3**), a "Trojan horse" conjugate produced by Streptomyces. (Bottom panel) Enterobactin–ciprofloxacin, mixed ligand biscatecholate–monohydroxamate siderophore–carbacephalosporin conjugate, **1b** and cefiderocol, FDA approved siderophore based "Trojan horse" antibiotic. Black: metal ion, red: siderophore, green: linker, blue: antibiotic.

concentration for 90% inhibition of growth (MIC_{90}) of 0.2, 1.9, 3.8 μM and 12.5 μM, respectively but fell short of exceeding the parent antibiotic's potency. Using a medicinal inorganic chemistry approach, we sought to further potentiate the activity of the construct.

Here, we introduce the second generation Trojan horse compound, Ga-**D5** (Galbofloxacin) as a ciprofloxacin-bearing mimic of albomycin natural product with a serine linker and explore its potential for a concerted diagnosis and therapy approach (Fig. 2). We incorporated a protease-sensitive serine linker in close analogy to the parent natural product albomycin.[31–34] We demonstrate that this structural modification is critical to further enhance the *in vitro* and *in vivo* antibiotic activity of Galbofloxacin against *S. aureus* beyond the potency of the parent antibiotic ciprofloxacin.

Experimental section

Materials and methods

All starting materials were purchased from Acros Organics, Alfa Aesar, Sigma Aldrich, or TCI America and used without further purification. NMR spectra (^1H and ^{13}C) were collected on a 700 MHz Advance III Bruker, 500 MHz or 400 MHz Bruker instrument at 25 °C and processed using TopSpin 3.5pl7. ^{19}F NMR were collected on a 400 MHz Bruker instrument at 25 °C using TFA as an internal standard (δ: −76 ppm). Chemical shifts are reported as parts per million (ppm). Mass spectrometry: low-resolution electrospray ionization (ESI) mass spectrometry and high-resolution (ESI) mass spectrometry was carried out at the Stony Brook University Institute for Chemical Biology and Drug Discovery (ICB&DD) Mass Spectrometry Facility with an Agilent LC/MSD and Agilent LC-UV-TOF spectrometers, respectively. UV-VIS spectra were collected with the NanoDrop 1C instrument (AZY1706045). Spectra were recorded from 190 to 850 nm in a quartz cuvette with 1 cm path length. HPLC: preparative HPLC was carried out using a Shimadzu HPLC-20AR equipped with a Binary Gradient, pump, UV-Vis detector, manual injector on a Phenomenex Luna C18 column (250 mm × 21.2 mm, 100 Å, AXIA packed). Method A (preparative purification method): A = 0.1% TFA in water, B = 0.1% TFA in MeCN. Gradient: 0–5 min: 95% A. 5–24 min: 5–95% B gradient. Method B (preparative purification method): A = 10 mM sodium acetate (pH = 4.5) in water, B = 100% MeCN. Gradient: 0–5 min: 95% A. 5–24 min: 5–95% B gradient. Analytical HPLC analysis was carried out using a Shimadzu HPLC-20AR equipped with a binary gradient, pump, UV-Vis detector, autoinjector and Laura radio detector on a Gemini-NX C18 column (100 mm × 3 mm, 110 Å, AXIA packed). Method C: A = 0.1% TFA in water, B = 0.1% TFA in MeCN with a flow rate of 0.8 mL min^{-1}, UV detection at 254 and 280 nm. Gradient: 0–2 min: 95% A. 2–14 min: 5–95% B gradient. 14–16 min: 95% B. 16–16.6 min: 95–5% B. 16.5–20 min: 5% B. Method D (analysis of ^{67}Ga/Ga complexes): A = 10 mM sodium acetate (pH = 4.5) in water, B = 100% MeCN. Gradient: 0–2 min: 95% A. 2–14 min: 5–95% B gradient. 14–16 min: 95% B. 16–16.6 min: 95–5% B. 16.5–20 min: 5% B, UV detection at 254 and 280 nm. Purity of all intermediates and final products including radiochemical

species was determined using analytical HPLC. All conjugates and complexes were ≥95% pure. ICP-OES was carried out using an Agilent 5110 ICP-OES. A 10-point standard with respect to gallium and iron was used and lines of best fit were found with R^2 of 0.999. IVIS Lumina Series II from Caliper LifeSciences small animal imager was used to image mice and *S. aureus* Xen 29 MIC plates. All scans were collected with blocked excitation filter, open emission filter (from 515 nm to 840 nm) and collection time $t = 5$ minutes. Images were analyzed with Living Image software version 4.3.1. Regions of interest were determined in quintuplicate with the ROI tool for each concentration as well as a general background ROI for background correction. 5-(*N*-Acetyl-*N*-acetoxyamino)-2-{5-(*N*-acetyl-*N*-acetoxy-amino)-2-[5-(*N*-acetyl-*N*-acetoxyamino)-2-(benzyloxy-carbonylamino) valerylamino]valerylamino}valeric acid (P5) and 7-(4-β-alanyl-1-piperazinyl)-1-cyclopropyl-6-fluoro-4-oxo-1*H*-quinoline-3-carboxylic acid (fragment A) were synthesized according to previously published procedures.[25] A detailed account of the chemical synthesis of **D5**, including NMR spectral assignments, HPLC traces, HRMS and corresponding data is provided in the ESI (Fig. S1–S17†).

Synthesis of coordination complexes of D5

Ga and Fe complexes of **D5** were synthesized using the following protocol. Galbofloxacin. **D5** (0.010 g, 0.009 mmol, 1 eq.) was dissolved in DMF (1 mL) and $Ga(NO_3)_3$ (0.007 g, 0.029 mmol, 3 eq.) dissolved in 10 mM CH_3COONa (pH = 5) was added. The pH of the solution was adjusted to 6 by adding 0.1 M NaOH. The reaction mixture was stirred for 1 h at 60 °C and overnight at room temperature. Solvent was removed *in vacuo* and product was purified by preparative HPLC (Method A, product elutes at 46% B) to afford Ga-**D5**/Galbofloxacin (0.006 g, 0.005 mmol, 62%) as a white solid. Calculated mass for Ga-**D5**/Galbofloxacin ($C_{44}H_{61}FGaN_{11}O_{15}$): 1071.3; found 1072.4 $[M + H]^+$. Retention time (method D): 7.13 min (purity/peak area: >99%). Fe-**D5**. **D5** (0.005 g, 0.004 mmol, 1 eq.) was dissolved in DMF (1 mL) and $FeCl_3$ (0.002 g, 0.012 mmol, 3 eq) was added. The reaction mixture was stirred for 1 h at room temperature. Solvent was removed *in vacuo* and product was purified by preparative HPLC (method A, product elutes at 48% B) to afford Fe-**D5** (0.006 g, 0.003 mmol, 87%) as a red solid. Calculated mass for Fe-**D5** ($C_{44}H_{61}FFeN_{11}O_{15}$): 1058.3; found 1059.3 $[M + H]^+$. Retention time (method D): 7.10 min (purity/peak area: >99%).

Antimicrobial activity assay

Antibacterial activity of *apo*-**D5**, its corresponding Fe and Ga complex and fragment A was determined by measuring their minimum inhibitory concentrations (MIC) using the broth microdilution method according to the Clinical and Laboratory Standards Institute (CLSI) guidelines. All aqueous solutions and media were prepared using deionized water. All liquids and media were sterilized by autoclaving (220 °C, 1 h) before use. Iron deficient Mueller–Hinton broth (MHB) (cation adjusted) was used for these assays. 5.25 g of MHB was added to 250 mL of deionized water. Aqueous solutions of 1 M Ca^{2+} (0.418 mL) and 1 M Mg^{2+} (0.155 mL) to 250 mL of MHB was added to the broth.

Edge Article

Chemical Science

The broth was autoclaved for 1 h at 220 °C. To make the broth iron-deficient, 4.06 mL of 1 mg mL^{-1} sterile (autoclaved) aq. solution of 2,2′-bipyridine (DP) was added to 250 mL of cation adjusted MHB. MIC experiments were conducted in triplicate and carried out at 3 different instances, resulting in $n = 9$ for each reported MIC$_{98}$, to ascertain a maximum error margin of <5% for each reported MIC value.

In general, 0.3 mM stock solutions of testing compounds were prepared. 10 μL solution of testing compound (0.3 mM) was added to the first well of the 96-well plate and serial dilutions were made down each row of the plate. 40 μL of growth media and 50 μL of diluted bacterial inoculum was also added to each well, resulting in a total volume of 100 μL and a concentration gradient of 0.3×10^{-4} M to 0.92×10^{-12} M. The dilution rate was adjusted keeping in mind the MIC of ciprofloxacin (positive control). The plates were incubated at 37 °C for 18 h and each plate was examined for bacterial growth using a plate reader (EPOCH2NS, Biotek microplate spectrometer). The MIC was recorded as the lowest compound concentration (μM) required to inhibit >90% of bacterial growth as judged by the absorbance of the culture media relative to the negative control.

Cytotoxicity experiments

HEK-293 cells were grown in MEM with 1% sodium pyruvate, 1% L-glutamine, 100 units per mL Pen Strep and 10% Fetal Bovine Serum. The cells were maintained at 37 °C in a humidified incubator under an atmosphere containing 5% CO$_2$. Modified Eagle's Medium (MEM), containing 10% fetal calf serum, 1% penicillin and streptomycin, was used as growth medium. HEK-293 cells were detached from the wells with trypsin and EDTA, harvested by centrifugation and resuspended again in cell culture medium. The assays were carried out on 96 well plates with 6000 cells per well for normal human embryonic kidney cells (HEK-293). After 24 h of incubation at 37 °C and 5% CO$_2$, the cells were treated with the compounds (with final DMSO concentrations of 0.5%) with a final volume of 200 mL per well. For a negative control, one series of cells was left untreated. The cells were incubated for 48 h followed by adding 50 mL MTT (2.5 mg mL^{-1}). After an incubation time of 2 h, the medium was removed and 200 mL of DMSO were added. The formazan crystals were dissolved, and the absorption was measured at 550 nm, using a reference wavelength of 620 nm. Each test was repeated in quadruplicates in three independent experiments. Results were plotted as % cell viability at different concentrations of samples tested.

$$\% \text{ Cell viability} = \frac{\text{OD}_{570} \text{ of test sample}}{\text{OD}_{570} \text{ of negative control}} \times 100$$

In vitro cleavability assessment

In vitro cleavage of **D5** and Galbofloxacin was performed using a proteinase K enzyme assay. Conjugates (10 μM) were incubated with proteinase K (20×, 200 μM, dissolved in Tris buffer, pH = 7) at 37 °C. Aliquots were removed at select time points, and were monitored for cleavage on analytical HPLC (**D5** – method C, Galbofloxacin – method D). Cleavage was confirmed by appearance of a second peak corresponding to the cleaved fragment A and was expressed as % cleavage over time.

Radiolabeling with ^{67}Ga and bacterial uptake of ^{67}Ga in wt bacterial strains

^{67}Ga-citrate was received from Jubilant Radiopharma at an average specific activity of 140.9 MBq mL^{-1}. The ^{67}Ga-citrate solution was converted to ^{67}Ga-chloride using a previously described protocol.[25] The average specific activity of the resultant ^{67}Ga-chloride solution used for radiolabeling was 131.3 MBq mL^{-1}. For radiolabeling of **D5**, an aliquot of (^{67}GaCl$_3$ 3.7 MBq, 30 μL) was mixed with a solution of **D5** (30 μL, 0.01 mM) in chelex resin treated water. The pH of the solution was adjusted with HEPES (100 mM, 100 μL) to 7.4. Complexation was monitored by radio-HPLC, method D. Radiolabeling was found to proceed after 5 minutes at room temperature. ^{67}Ga–**D5**: t_R = 7.13 min (purity/peak area: 99%).

Wt E. coli (Mg 1655), wt S. aureus (RN4220) and wt P. aeruginosa (PAO1) were grown overnight in 5 mL LB (Fe-deficient) at 37 °C. The overnight cultures were inoculated in 10 mL iron deficient LB and incubated at 37 °C until the OD$_{600}$ reached 0.4. Uptake was initiated by adding ^{67}Ga complexes (10 μL, 0.18 MBq) to culture tubes containing 10 mL bacterial inoculum and incubating at 37 °C. Aliquots (1 mL) were removed after 10 min, 20 min, 30 min, 1 h and 2 h and centrifuged for 3 min (34 000 rpm). The supernatant was removed, and the bacterial pellet was washed with DPBS (1 mL, 3×). The assay was performed in five replicates and in parallel with a ^{67}Ga-citrate control. All tubes were counted using an automated gamma counter to quantify retained radioactivity in pellets in comparison to the 1 mL parent inoculum.

To challenge active transporter-mediated uptake, the bacterial cultures were preincubated with 200× Fe-LDFC. ^{67}Galbofloxacin (10 μL, 0.18 MBq) was added after 30 min. Aliquots (1 mL) were removed after 10 min, 20 min, 30 min, 1 h and 2 h and centrifuged for 3 min. Pellet were washed with DPBS (3×) and retained activity was quantified as described above.

Biodistribution of naïve and infected Balb/c mice

All animal experiments were performed using protocols approved by the Institutional Animal Care and Use Committee (IACUC) at Stony Brook University accredited through Association for Assessment and Accreditation of Laboratory Animal Care International (AAALAC International, Federal assurance #A3011-01). 0.3–0.6 MBq of ^{67}Galbofloxacin and ^{67}Ga-citrate (control) were intravenously injected via tail vein catheter in naïve mice. Mice were sacrificed 1 h p.i. and select organs were harvested. Radioactivity was counted by using a gamma counter, and the radioactivity associated with each organ was expressed as % ID g^{-1}. For infected mice biodistribution, mice were given a S. aureus (10^5 CFU, 50 μL) in left triceps. After 1 h p.i. mice were sacrificed and select organs were harvested. Radioactivity was counted by using a gamma counter, and the

radioactivity associated with each organ was expressed as % ID g^{-1}.

Metabolite analysis

100 μL of urine was directly injected on the radio HPLC. Eluate was collected in 30 s increments from 0–15 minutes. Activity in each tube was quantified using a gamma counter. The counts were used to reconstruct the metabolite trace which was then compared to the HPLC traces of the original ^{67}Galbofloxacin complex.

Galbofloxacin efficacy study

All animal experiments were conducted according to the guidelines of the Institutional Animal Care and Use Committee (IACUC) at Stony Brook Medicine. Bacterial stocks were freshly prepared before inoculation. In general, bioluminescent *S. aureus* Xen 29 strain was cultured in MHB at 37 °C to mid log phase ($OD_{600} = 0.4$, 2×10^8 cells per mL). Bacterial cells were harvested by centrifugation (34 000 rpm, 3 min) and washed with sterilized MHB. Final inoculums were generated by diluting bacteria to the desired concentrations in MHB. To induce localized infection model, mice were injected with 2×10^7 bacterial cells (2×10^8 cells per mL inoculum, 50 μL) into the left forelimb muscle of mice. Test compounds were administered intravenously 1 h and 25 hours post bacterial inoculation. The study included five groups of mice: ciprofloxacin as positive control: 284.4 μmol kg^{-1} (4 mice) and 9.3 μmol kg^{-1} (4 mice); vehicle (saline) as a negative control (4 mice); and Galbofloxacin: 9.3 μmol kg^{-1} (4 mice) and 2.3 μmol kg^{-1} (4 mice). Muscle size and survival was monitored for 7 days post-infection. The mice were also imaged on a small animal imager every 12 hours for 7 days to monitor the infection burden and treatment efficacy. After 7 days, mice were euthanized, infected and control muscle from each cohort was extracted and plated for CFU determination.

Results and discussion

Synthesis of siderophore antibiotic conjugate D5 and its metal complexes: galbofloxacin and Fe-D5

The structure of **D5** draws direct structural inspiration from the natural product albomycin; the presence of the serine linker is essential for the release of the *t*-seryl transferase inhibitor portion of the natural product inside the bacterial cytoplasm.[31,35–37] Thus, we proposed that the introduction of serine to our ciprofloxacin-conjugates could result in enhanced efficacy by way of drug cargo release, a concept validated by Nolan and coworkers on enterobactin derived constructs.[34,38] We implemented a conjugation strategy mirroring the connectivity of the natural product albomycin and our first-generation lead **D2**. The acetylated, amino protected linear desferrichrome precursor P5 was obtained by employing the synthetic strategy pioneered by Miller and coworkers.[25,39–41] The serine linker was introduced to the building block P5 by functionalizing ciprofloxacin first with Fmoc-β-alanine,[38] followed by N-terminal deprotection and subsequent reaction of the free amine of

fragment A[25] with Fmoc-Ser(O^{t}Bu)-OH with 2-(1*H*-benzotriazol-1-yl)-1,1,3,3-tetramethyluronium hexafluorophosphate, Hexafluorophosphate Benzotriazole Tetramethyl Uronium (HBTU) mediated amidation using a solution phase coupling approach. A second amidation step with the protected, linear desferrichrome-derived building block P5 following Fmoc-deprotection of the serine residue (Scheme S1†) was employed to link the proto-siderophore P5 with the drug cargo precursor (2). The final product **D5** was attained in a <2% over-all yield after 16 steps following final purification using reverse phase chromatography (Fig. S1–S17†).

Complexation of **D5** with Ga(III) and Fe(III) salts formed Galbofloxacin and Fe-**D5** in aqueous, buffered media at pH 6 and pH 7, respectively. The corresponding complexes were further purified using reverse phase chromatography and isolated as white and orange-red powders, respectively. Characterization *via* high performance liquid chromatography (HPLC), high resolution mass spectrometry (HRMS) and inductive coupled plasma-optical emission spectrometry (ICP-OES) was employed to affirm purity and produce consistent complex concentrations for subsequent *in vitro* and *in vivo* studies based on the quantitation of metal content (Fig. S5, S6, S16 and S17†).

Growth inhibition in *wt* bacterial strains

With *apo*- (metal-free), Ga and Fe complexes of **D5** in hand, we next probed their ability to inhibit bacterial growth in a conventional minimum inhibitory concentration for 98% inhibited growth (MIC_{98}) assay. We selected *E. coli* K12 and *P. aeruginosa* PA01 as Gram-negative model organisms, and *S. aureus* RN4220 as the Gram-positive model organism. Fe-deficient media was prepared by addition of 2,2′-bipyridine (DP) to mimic the tightly iron controlled *in vivo* environment.[15,42,43] The parent drug ciprofloxacin was utilized as a control giving an MIC_{98} of 0.93 μM, which is consistent with literature values. *apo*-**D5** and Galbofloxacin were determined to have MIC_{98} of 0.93 μM in wt *E. coli*, retaining the growth inhibitory action of ciprofloxacin and comparable to the antibiotic activity of our first-generation conjugate Ga-**D2**. In accordance with our previous findings, Fe(III) complexes remain significantly less active: Fe-**D5** showed a 2-fold decrease in activity in *E. coli* in comparison to *apo*-**D5** and Galbofloxacin. We hypothesize that the concerted delivery of Fe at elevated concentrations is growth promoting and efficiently offsets the inhibitory action of the siderophore-mediated delivery of the

Table 1 Summary of MIC_{98} (μM) determined in *E. coli*, *S. aureus* and *P. aeruginosa*. GP: growth promoting

Compound	*E. coli*	*S. aureus*	*PA01*
Ciprofloxacin	0.93 ± 0.00	0.93 ± 0.00	0.93 ± 0.00
apo-**D5**	0.93 ± 0.02	0.93 ± 0.00	30 ± 0.04
Galbofloxacin	0.93 ± 0.00	0.093 ± 0.00	15 ± 0.03
Fe-**D5**	1.9 ± 0.02	7.5 ± 0.00	GP
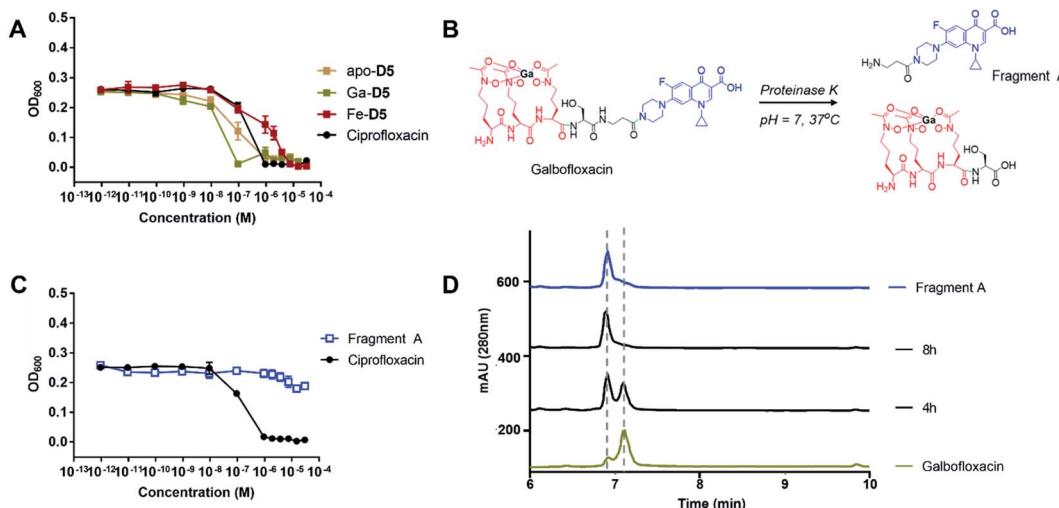
Fig. 3 (A) MIC assay of Galbofloxacin in *S. aureus* shows that the Galbofloxacin complex exhibits an order of magnitude higher potency when compared to ciprofloxacin, while *apo*-D5 and Fe-D5 exhibit similar or attenuated growth inhibition respectively, when compared to ciprofloxacin ($n = 3 \times 3$). (B) Schematic description of proteinase K assay with Galbofloxacin at 37 °C, pH 7. (C) MIC assay of cleaved fragment A in *S. aureus* shows no growth inhibitory activity for fragment A ($n = 3 \times 3$). (D) *In vitro* assay using proteinase K shows time dependent cleavage of Galbofloxacin ($t_R = 7.13$ min) by appearance of a second peak corresponding to the cleaved fragment A ($t_R = 7.03$ min) ($n = 2$).

ciprofloxacin payload (Fig. S18,† Table 1). In *P. aeruginosa,* the activity of *apo*-D5 and Galbofloxacin activity decreased 10-fold with an MIC_{98} value of 30 μM and 15 μM respectively, while Fe-D5 produced growth promoting effects (Fig. S18,† Table 1). However, *S. aureus* exhibited exceptional sensitivity to Galbofloxacin with an MIC_{98} of 93 nM, an order of magnitude higher activity than parent drug ciprofloxacin (Fig. 3A, Table 1). This qualifies Galbofloxacin as one of the most active synthetic Trojan horse compounds against *S. aureus* measured to date. The *apo*-D5 compound showed and MIC_{90} of 0.93 μM, whereas Fe-D5 showed decreased activity ($MIC_{90} = 7.5$ μM) (Fig. 3A, Table 1), indicating that complexation with Ga(III) is essential to produce the synergistic, growth inhibitory effect.

D5 and its metal complexes were also accessed for its antimicrobial activity in the FhuA transporter deficient mutant *E. coli* AN193. Fig. S19† summarizes the corresponding results: the previously observed growth inhibitory activity in *E. coli* of *apo*-D5, Galbofloxacin and Fe-D5 is completely muted, while ciprofloxacin retains its growth inhibitory activity as found with the wt *E. coli* strain. This demonstrates that internalization and activity of Galbofloxacin remains FhuA-dependent, affirming that siderophore-mediated active transport of D5-constructs remains essential to produce growth inhibition.

In vitro cleavage of galbofloxacin and *apo*-D5

As growth inhibition experiments confirmed that Galbofloxacin exhibited increased potency, we assessed *apo*-D5 and Galbofloxacin as substrates for proteinase mediated cleavage adjacent to the serine residue. *In vivo*, the antibacterial active moiety is released by peptidase N.[31,32] The same reaction can be mimicked *in vitro* by proteinase K,[44,45] a broad-spectrum serine protease (Fig. 3B). We incubated 10 μM of *apo*-D5 ($t_R = 7.28$ min), Fe-D5 ($t_R = 6.96$ min) or Galbofloxacin ($t_R = 7.13$ min)

with proteinase K (20×, 200 μM, in tris buffer, pH = 7) at 37 °C and monitored cleavage by analytical HPLC, which reveals release of fragment A ($t_R = 7.03$ min, Fig. 3B and D). Under these conditions, proteinase K cleaved *apo*-D5 completely in 15 min (Fig. S21, Table S1†), whereas the cleavage for Galbofloxacin is slower, with a $t_{1/2}$ of 4 h, with complete cleavage to fragment A after 8 h (Fig. 3D, Table S1†). The cleavage of Fe-D5 was slowest with 34% conjugate still intact after 24 h incubation with proteinase K (Fig. S21,† Table S1†). The results for *apo*-D5, Fe-D5 and Galbofloxacin are consistent with prior enzymatic cleavage studies on albomycin and desferri-albomycin.[44] The results also indicate higher dissociation constant for Fe-D5 as compared with Galbofloxacin.

While *apo*-D5, Fe-D5 and Galbofloxacin are proteinase substrates, it is conceivable that dissociation of the metal ion in the bacterial cytoplasm results in accelerated cleavage of the conjugate to release the antibacterial payload. Importantly, cleavage of the construct does not occur outside the bacterial envelope, as fragment A is completely inactive in all tested *wt* bacterial strains (*E. coli*, *S. aureus* and *P. aeruginosa*, Fig. 3C and S20†). These results affirm the importance of siderophore mediated active uptake of Galbofloxacin prior to release of the antibiotic payload.

Cytotoxicity analysis

As we had identified Galbofloxacin as a potent antibiotic against *S. aureus*, and with potential for prospective *in vivo* applications, we explored its toxicity to mammalian cells next. Specifically, we determined the anti-proliferative activity of Galbofloxacin and *apo*-D5 against normal human embryonic kidney cells (HEK-293) using cisplatin, gallium(III) citrate and ciprofloxacin as controls. As indicated in Fig. 4, the Galbofloxacin conjugate displays no *in vitro* toxicity up to 80 μM, with a slightly reduced
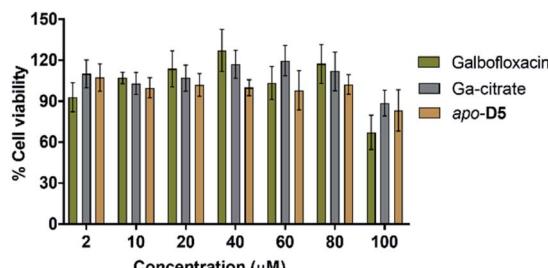
Fig. 4 MTT assay of Galbofloxacin, *apo*-D5 and Ga-citrate in HEK-293 cell line shows low cytotoxicity for all tested conjugates ($n = 3 \times 5$).

cell viability (85%), comparable to ciprofloxacin, at 100 μM (Fig. S22†). In comparison, the benchmark cytotoxin cisplatin produces reduced cell viability of 60% at 2 μM compound concentration (Fig. S22†). *apo*-D5 and Ga(III) citrate are nontoxic to HEK-293 human cells at all tested concentrations (Fig. 4).

Radiochemical labeling with ^{67}Ga and radiochemical uptake experiments in *wt* bacterial strains

We next employed a radiochemical tracer approach to further elucidate and quantitate *in vitro* and *in vivo* properties of Galbofloxacin. To this end, we employed ^{67}Ga ($t_{1/2}$ = 79 hours, E_γ (avg) = 93.3 keV), an isotope with multi-day half-life that enables bacterial uptake and pharmacokinetic studies. The formation of the ^{67}Galbofloxacin complex is feasible under mild radiolabeling conditions (pH 7, 100 mM HEPES, 5 minutes) (Fig. 5A) quantitatively with ligand concentrations of 10^{-6} M. The complexation was monitored using a radio-HPLC (Fig. 5B, method D).

The radiolabeled ^{67}Galbofloxacin complex provides a convenient tool to probe time-dependent compound uptake in bacteria relative to weakly complexed ^{67}Ga-citrate. ^{67}Galbofloxacin was prepared as outlined previously, with an average specific activity of 1.9 MBq μmol^{-1}. *E. coli*, *S. aureus* and *P. aeruginosa* (3.2×10^8 CFU) were incubated in Fe-deficient LB with 0.18 MBq of ^{67}Galbofloxacin at 37 °C. Aliquots were removed at 10, 20, 30, 60 and 120 minutes followed by separation of pellets from supernatant and counting of retained radioactivity in each fraction. For all the tested strains, ^{67}Galbofloxacin shows time dependent increase in uptake with a peak uptake at 120 minutes and statistically significant, enhanced uptake in comparison to ^{67}Ga-citrate, for *E. coli* and *P. aeruginosa* (Fig. S23, S24, Tables S2 and S3†). Notably, for *S. aureus*, ^{67}Galbofloxacin uptake was comparable to ^{67}Ga-citrate uptake (Fig. 5C, Table S4†). We hypothesize that ^{67}Ga-citrate is efficiently taken up by *S. aureus* due to its similarity to staphyloferrin, a citric acid based siderophore naturally produced by *S. aureus*.[46] To probe siderophore specific active transport to the bacterial cytoplasm, we also challenged ^{67}Galbofloxacin uptake with the Fe complex of parent siderophore (Fe-LDFC). All three bacterial cultures were incubated for 30 min with 200× excess Fe-LDFC before addition of ^{67}Galbofloxacin. We observed statistically significant depression of ^{67}Galbofloxacin uptake within the bacterial pellet at all time points (Fig. 3D, S25, S26, Tables S5, S6 and S7†).

In vivo biodistribution and pharmacokinetics in naïve and infected mice models

With ^{67}Galbofloxacin uptake validated *in vitro* using bacterial uptake assays, we investigated biodistribution ^{67}Galbofloxacin *in vivo* next. Balb/c mice (female, 8 weeks) were injected with
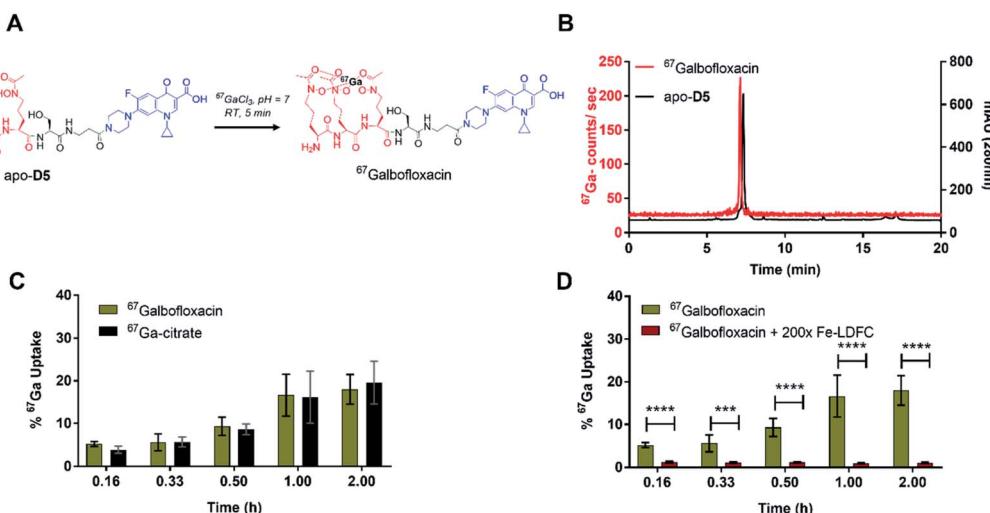
Fig. 5 (A) Schematic description of the radiochemical complexation of *apo*-D5 with ^{67}Ga. ^{67}Ga-complexation proceeds in 5 min, 25 °C, pH 7. (B) A representative radiolabeing HPLC trace for the characterization of ^{67}Galbofloxacin (t_R = 7.13 min, left axis, ^{67}Ga counts per second), in comparison with HPLC characterization of the *apo*-D5 ligand (t_R = 7.28 min, right axis, absorbance at 280 nm) is shown. Free ^{67}Ga elutes at 0.7 minutes. (C) Time-dependent, radiochemical bacterial uptake studies in *S. aureus* of ^{67}Galbofloxacin in iron deficient, DP-treated media show that uptake is comparable with ^{67}Ga-citrate, which acts as a staphyloferrin (natural siderophore) mimic for *S. aureus* ($n = 5$). (D) On pre-incubation with 200× Fe-LDFC, the uptake of ^{67}Galbofloxacin in *S. aureus* is attenuated significantly after 10 min ($n = 5$).
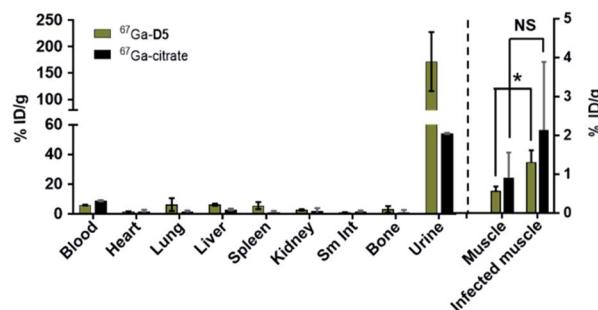
Fig. 6 Comparative biodistribution of [67]Galbofloxacin and ^{67}Ga-citrate in naïve mice ($n = 3$) shows predominantly renal clearance. (Right to the dotted line) Comparative biodistribution of [67]Galbofloxacin and ^{67}Ga-citrate in *S. aureus* infected mice ($n = 3$), [67]Galbofloxacin shows a significant higher uptake ($P \leq 0.05$) in the infected muscle as compared to the control muscle ($n = 3$).

[67]Galbofloxacin and ^{67}Ga-citrate intravenously, followed by biodistribution and analysis of metabolites in the urine using radio-HPLC at 1 hour post injection. Naïve biodistribution revealed rapid, renal clearance of all both [67]Galbofloxacin and ^{67}Ga-citrate (Fig. 6, Table S8†). Metabolite study revealed 5% intact [67]Galbofloxacin radiochemical complex in the urine (Fig. S27†). To quantitate the bacterial uptake of [67]Galbofloxacin *in vivo*, we induced a localized, soft tissue infection in mice using 10^5 CFU *S. aureus* infection in the left triceps. [67]Galbofloxacin showed a significant, enhanced uptake ($P \leq 0.05$) in the infected muscle as compared to the control muscle (Fig. 6, Table S8†), in contrast to ^{67}Ga-citrate, which did not distinguish infected and control muscle tissues. Overall,

favorable pharmacokinetics, as indicated by rapid renal excretion, no significant off-target organ uptake, and increased uptake in infected muscle qualifies [67]Galbofloxacin for further evaluation for therapy in an animal model of soft tissue infection.

Growth inhibition in bioluminescent *S. aureus* strain Xen 29 and *in vivo* therapy studies

The bioluminescent *S. aureus* strain Xen 29 has previously been used to monitor *in vivo* antibiotic efficacy using preclinical bioluminescence imaging non-invasively.[47–50] Therefore, before using *S. aureus* Xen 29 for *in vivo* therapy studies, the *in vitro* antibacterial activity of Galbofloxacin was accessed in *S. aureus* Xen 29. MIC assays were performed in Fe deficient media as described for the *wt* strains. The parent drug ciprofloxacin was employed as a control with MIC_{98} of 3.8 μM. Galbofloxacin exhibits MIC_{98} of 0.93 μM, 4× more potent than ciprofloxacin. The 96 well plates for both ciprofloxacin and Galbofloxacin were imaged on small animal optical imager (Fig. 7A and C) to quantify the radiance value due to the bioluminescent bacteria for each well. The MIC results based on OD_{600} and ROI analysis coincided for both test compounds as shown in Fig. 7B and D. The 4-fold higher activity of Galbofloxacin as compared to ciprofloxacin in *S. aureus* Xen 29 affirmed this strain as an ideal model system for *in vivo* therapy studies.

The *in vivo* therapeutic activity of Galbofloxacin was evaluated in *S. aureus* Xen 29 triceps infection model. 8 week-old female Balb/c mice were infected intramuscularly with 2×10^7 bacterial cells in the left forelimb and treatments were administered intravenously at 1 h and 25 h post infection. The
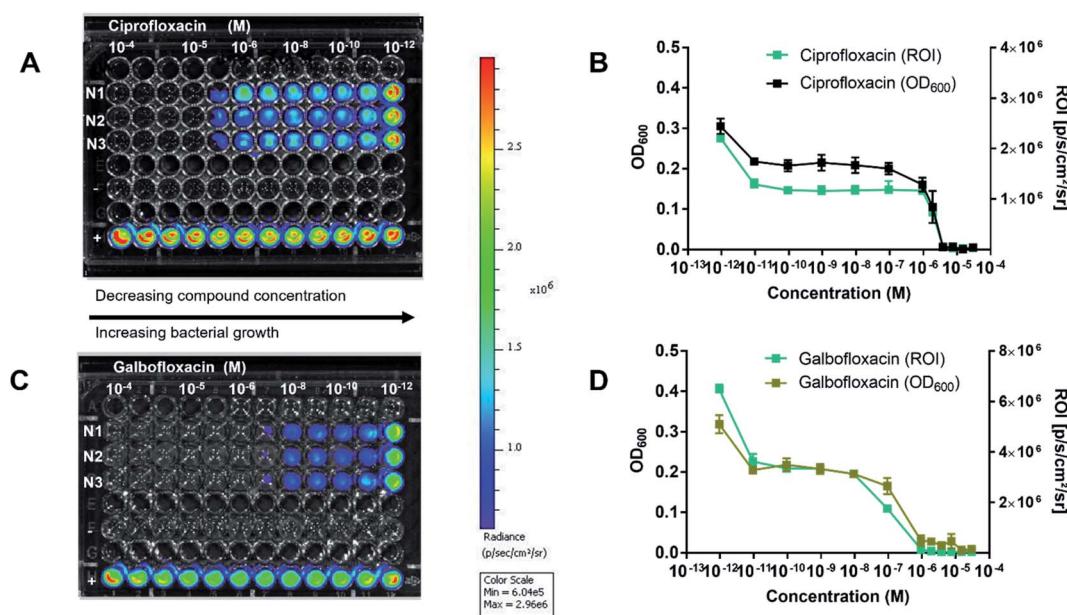
Fig. 7 (A) Bioluminescence image of ciprofloxacin 96 well plate tested in *S. aureus* Xen 29 and imaged on an IVIS small animal scanner. (B) MIC assay results of ciprofloxacin in *S. aureus* Xen 29 (left axis, OD_{600}), in comparison with bioluminescence characterization (right axis, radiance) is shown ($n = 3 \times 3$). (C) Bioluminescence image of Galbofloxacin 96 well plate tested in *S. aureus* Xen 29 and imaged on an IVIS small animal scanner. (D) MIC assay results of Galbofloxacin in *S. aureus* Xen 29 (left axis, OD_{600}), in comparison with bioluminescence characterization (right axis, radiance) is shown ($n = 3 \times 3$).
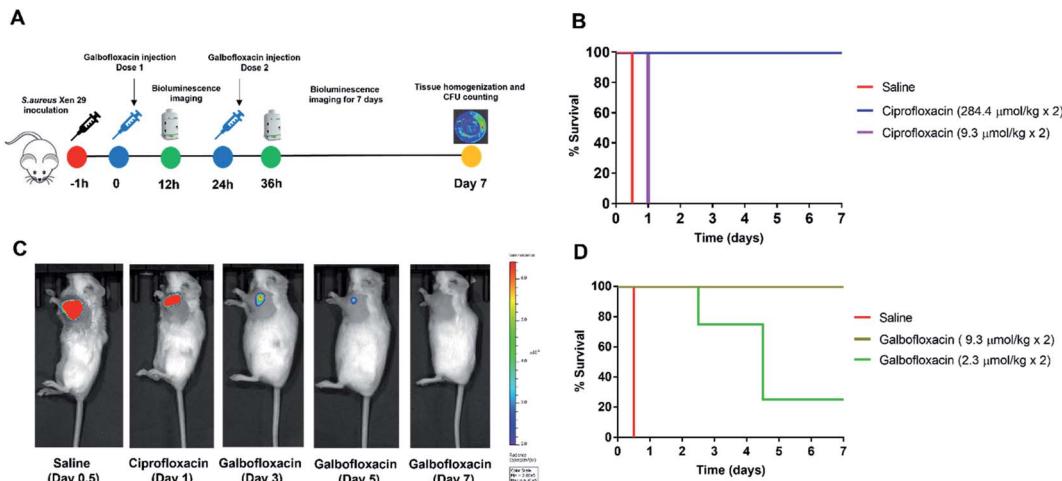
Fig. 8 (A) *In vivo* therapy experimental timeline. (B) Survival plot showing 100% survival for ciprofloxacin (284.4 μmol kg^{-1}) after 7 days, whereas mice dosed with 9.3 μmol kg^{-1} ciprofloxacin were euthanized on day 1. Saline mice were euthanized after 12 h. (C) Bioluminescence imaging of mice dosed with vehicle (saline), ciprofloxacin (9.3 μmol kg^{-1}) and Galbofloxacin (9.3 μmol kg^{-1}). (D) Survival plot showing 100% survival for Galbofloxacin (9.3 μmol kg^{-1}) after 7 days, whereas % survival was 25% for mice dosed with 2.3 μmol kg^{-1} Galbofloxacin after 7 days. Saline mice were euthanized after 12 h due to meeting study endpoint criteria of muscle enlargement and distress.

Table 2 Summary of therapy study results

Compound (dose)	Single dose (mg kg^{-1})	Single dose (μmol kg^{-1})	Max survival (day 7)	CFU per mL (average)
Saline	—	—	0/4	1.58 x 10^{11}
Ciprofloxacin (high dose)	94.2	284.4	4/4	0
Ciprofloxacin (medium dose)	3.5	9.3	0/4	8.86 x 10^{8}
Galbofloxacin (medium dose)	10	9.3	4/4	0
Galbofloxacin (low dose)	2.5	2.3	1/4	3.60 x 10^{5}

treatments included 4 mice in each cohort of ciprofloxacin high dose (284.4 μmol kg^{-1}), ciprofloxacin medium dose (9.3 μmol kg^{-1}), Galbofloxacin medium dose (9.3 μmol kg^{-1}), Galbofloxacin low dose (2.3 μmol kg^{-1}) and vehicle (saline) (Table S9†). Mice were imaged on a small animal optical imager every 12 hours and monitored for change in muscle size and survival (Fig. 8A) for 7 days. The muscle size for the vehicle and ciprofloxacin (9.3 μmol kg^{-1}) increased rapidly, for Galbofloxacin (2.3 μmol kg^{-1}) it increased gradually, whereas for ciprofloxacin (284.4 μmol kg^{-1}) and Galbofloxacin (9.3 μmol kg^{-1}) cohort the muscle size decreased over the course of 7 days (Fig. S28 and S29†). Bioluminescence imaging and ROI analysis revealed increased and eventually fatal infection for ciprofloxacin (9.3 μmol kg^{-1}) on day 1 (Fig. 8C, S31, S40, Table S10†), whereas the infection burden decreased for Galbofloxacin (9.3 μmol kg^{-1}) over the course of 7 days (Fig. 8C, S47, S44, Table S10†) and efficiently reduced morbidity. Untreated mice had a survival of 0% after 12 h (Fig. 8B–D, S40,† Tables 2 and S10†). Infected muscle from each cohort was plated after euthanizing and infection burden was determined by counting the CFUs (Fig. S39,† Table 2) and imaging the agar plates on IVIS scanner (Fig. S30, S32, S34, S36 and S38†). Mice treated with medium

dose ciprofloxacin (9.3 μmol kg^{-1}) had a survival of 0% after day 1 (Fig. 8C, Table 2), whereas the survival was 100% for same dose Galbofloxacin mice at day 7 (Fig. 8D, Table 2).

Mice receiving Galbofloxacin at 2.3 μmol kg^{-1} dose exhibited increased survival, albeit infection persisted. By day 4.5 the low dose Galbofloxacin cohort showed slowed progression of infection when compared to the vehicle treated cohort (Fig. S35†). The survival rate was 25% on day 7 for mice dosed with 2.3 μmol kg^{-1} Galbofloxacin (Fig. 8D, Table 2). Mice dosed with ciprofloxacin (284.4 μmol kg^{-1}) survived for 7 days and showed efficient reduction of infection, indicating expected dose dependency (Fig. 8C, S33,† Table 2).

Conclusions

Here, we show for the first time that a Ga-siderophore antibiotic conjugate, Galbofloxacin exhibits both superior *in vitro* potency and *in vivo* efficacy when compared to its parent antibiotic ciprofloxacin. In our study, Galbofloxacin shows an order of magnitude higher potency in comparison to the parent drug ciprofloxacin against *S. aureus* with MIC$_{98}$ of 93 nM. Moreover, Galbofloxacin shows higher potency than *apo*-**D5** (MIC$_{98}$ = 0.93

μM) indicating the synergistic effect of Ga complexation, siderophore-mediated transmembrane transport and cytoplasmic release of the antibiotic. MIC assay with FhuA deficient *E. coli* results in no growth inhibition, demonstrating siderophore mediated active uptake remains essential for Galbofloxacin. MTT assay in HEK-293 cells demonstrates no toxicity for Galbofloxacin up to 80 μM, comparable to ciprofloxacin at 100 μM. Proteinase K assay was carried out to demonstrate the time dependent, proteolytic cleavage of Galbofloxacin. The results indicate 50% cleavage of Galbofloxacin after 4 h in the presence of 20× proteinase K. We also quantified bacterial uptake for the conjugate and measured *in vivo* pharmacokinetics using ^{67}Galbofloxacin. ^{67}Galbofloxacin can be synthesized radiochemically under mild conditions and with high radiochemical yields. The complex shows time dependent siderophore mediated active uptake in *wt* bacterial strains. Biodistribution of ^{67}Galbofloxacin in naïve mice and in a mouse model of intramuscular infection reveals renal clearance and significantly enhanced uptake in infected muscle when compared to ^{67}Ga-citrate, which showed no difference. Finally, an *in vivo* therapy study with Galbofloxacin in a *S. aureus* Xen 29 murine infection model demonstrates that the high *in vitro* potency of Galbofloxacin is directly reflective of its *in vivo* efficacy. Mice dosed twice with 9.3 μmol kg^{-1} of Galbofloxacin survived for 7 days with the infection burden decreasing and eventually resolving completely over the course of study, whereas the infection burden was fatal on day 1 for mice dosed with same molar dose of ciprofloxacin.

Galbofloxacin constitutes the first, rationally designed gallium coordination complex with superior potency to combat Gram-positive soft tissue infection when compared to its parent antibiotic. Galbofloxacin also demonstrates that Trojan horse antibiotics can successfully reprise their *in vitro* potency *in vivo*. The expansion of the scope of treatable infections by modification of the metal, antibiotic payload as well as mechanistic studies to further elucidate the potentiating, growth inhibitory effect of Ga-sideromycins on bacterial cells are underway.

Data availability

All experimental and image data is shown in the ESI,† and additional raw data files can be obtained from the authors upon request.

Author contributions

Experiments were designed by AP and EB, experiments were conducted by contributions from authors. The manuscript was written and edited by all authors.

Conflicts of interest

There are no conflicts to declare.

Acknowledgements

References

1 CDC, *Biggest Threats and Data | Antibiotic/Antimicrobial Resistance*, CDC, 2019.
2 Y. Guo, G. Song, M. Sun, J. Wang and Y. Wang, *Front. Cell. Infect. Microbiol.*, 2020, **10**, 107.
3 S. Y. C. Tong, J. S. Davis, E. Eichenberger, T. L. Holland and V. G. Fowler, *Clin. Microbiol. Rev.*, 2015, **28**, 603–661.
4 S. Y. C. Tong, J. S. Davis, E. Eichenberger, T. L. Holland and V. G. Fowler, *Clin. Microbiol. Rev.*, 2015, **28**, 603–661.
5 R. J. Turner, *Microbiol. Biotechnol.*, 2017, **10**, 1062–1065.
6 A. Pandey and E. Boros, *Chem.–Eur. J.*, 2021, **27**, 7340–7350.
7 U. E. Schaible and S. H. E. Kaufmann, *Nat. Rev. Microbiol.*, 2004, **2**, 946–953.
8 T. A. Wencewicz and M. J. Miller, *Top. Med. Chem.*, 2018, **26**, 151–183.
9 R. C. Hider and X. Kong, *Nat. Prod. Rep.*, 2010, **27**, 637–657.
10 G. L. A. Mislin and I. J. Schalk, *Metallomics*, 2014, **6**, 408–420.
11 C. Ji, R. E. Juárez-Hernández and M. J. Miller, *Future Med. Chem.*, 2012, **4**, 297–313.
12 S. C. Andrews, A. K. Robinson and F. Rodríguez-Quiñones, *FEMS Microbiol. Rev.*, 2003, **27**, 215–237.
13 M. J. Miller, H. Zhu, Y. Xu, C. Wu, A. J. Walz, A. Vergne, J. M. Roosenberg, G. Moraski, A. A. Minnick, J. McKee-Dolence, J. Hu, K. Fennell, E. Kurt Dolence, L. Dong, S. Franzblau, F. Malouin and U. Möllmann, *BioMetals*, 2009, **22**, 61–75.
14 T. A. Wencewicz and M. J. Miller, *J. Med. Chem.*, 2013, **56**, 4044–4052.
15 T. Zheng and E. M. Nolan, *J. Am. Chem. Soc.*, 2014, **136**, 9677–9691.
16 H. K. Zane, H. Naka, F. Rosconi, M. Sandy, M. G. Haygood and A. Butler, *J. Am. Chem. Soc.*, 2014, **136**, 5615–5618.
17 J. A. Karlowsky, M. A. Hackel, M. Tsuji, Y. Yamano, R. Echols and D. F. Sahm, *Int. J. Antimicrob. Agents*, 2019, **53**, 456–466.
18 T. Aoki, H. Yoshizawa, K. Yamawaki, K. Yokoo, J. Sato, S. Hisakawa, Y. Hasegawa, H. Kusano, M. Sano, H. Sugimoto, Y. Nishitani, T. Sato, M. Tsuji, R. Nakamura, T. Nishikawa and Y. Yamano, *Eur. J. Med. Chem.*, 2018, **155**, 847–868.
19 G. G. Zhanel, A. R. Golden, S. Zelenitsky, K. Wiebe, C. K. Lawrence, H. J. Adam, T. Idowu, R. Domalaon, F. Schweizer, M. A. Zhanel, P. R. S. Lagacé-Wiens, A. J. Walkty, A. Noreddin, J. P. Lynch III and J. A. Karlowsky, *Drugs*, 2019, **79**, 271–289.
20 J. Y. Wu, P. Srinivas and J. M. Pogue, *Infect. Dis. Ther.*, 2020, **9**, 17–40.
21 W. Neumann, M. Sassone-Corsi, M. Raffatellu and E. M. Nolan, *J. Am. Chem. Soc.*, 2018, **140**, 5193–5201.

22 T. J. Sanderson, C. M. Black, J. W. Southwell, E. J. Wilde, A. Pandey, R. Herman, G. H. Thomas, E. Boros, A.-K. Duhme-Klair and A. Routledge, *ACS Infect. Dis.*, 2020, **6**, 2532–2541.

23 M. Ghosh, Y. M. Lin, P. A. Miller, U. Möllmann, W. C. Boggess and M. J. Miller, *ACS Infect. Dis.*, 2018, **4**, 1529–1535.

24 M. Ghosh, P. A. Miller, U. Möllmann, W. D. Claypool, V. A. Schroeder, W. R. Wolter, M. Suckow, H. Yu, S. Li, W. Huang, J. Zajicek and M. J. Miller, *J. Med. Chem.*, 2017, **60**, 4577–4583.

25 A. Pandey, C. Savino, S. H. Ahn, Z. Yang, S. G. Van Lanen and E. Boros, *J. Med. Chem.*, 2019, **62**, 9947–9960.

26 C. E. Arnold, A. Bordin, S. D. Lawhon, M. C. Libal, L. R. Bernstein and N. D. Cohen, *Vet. Microbiol.*, 2012, **155**, 389–394.

27 C. R. Chitambar, *Biochim. Biophys. Acta, Mol. Cell Res.*, 2016, **1863**, 2044–2053.

28 C. H. Goss, Y. Kaneko, L. Khuu, G. D. Anderson, S. Ravishankar, M. L. Aitken, N. Lechtzin, G. Zhou, D. M. Czyz, K. McLean, O. Olakanmi, H. A. Shuman, M. Teresi, E. Wilhelm, E. Caldwell, S. J. Salipante, D. B. Hornick, R. J. Siehnel, L. Becker, B. E. Britigan and P. K. Singh, *Sci. Transl. Med.*, 2018, **10**, eaat7520.

29 C. Goss, D. Hornick and M. Aitken, *Pediatr. Pulmonol.*, 2012, **47**, 303.

30 Y. Wang, B. Han, Y. Xie, H. Wang, R. Wang, W. Xia, H. Li and H. Sun, *Chem. Sci.*, 2019, **10**, 6099–6106.

31 Z. Lin, X. Xu, S. Zhao, X. Yang, J. Guo, Q. Zhang, C. Jing, S. Chen and Y. He, *Nat. Commun.*, 2018, **9**, 3445.

32 G. F. Gause, *Br. Med. J.*, 1955, **2**, 1177–1179.

33 T. E. Clarke, V. Braun, G. Winkelmann, L. W. Tari and H. J. Vogel, *J. Biol. Chem.*, 2002, **277**, 13966–13972.

34 Z. L. Reitz, M. Sandy and A. Butler, *Metallomics*, 2017, **9**, 824–839.

35 V. Braun, K. Gunthner, K. Hantke and L. Zimmermann, *J. Bacteriol.*, 1983, **156**, 308–315.

36 A. Pramanik, U. Stroeher, J. Krejci, A. Standish, E. Bohn, J. Paton, I. Autenrieth and V. Braun, *Int. J. Med. Microbiol.*, 2007, **297**, 459–469.

37 A. Hartmann, H. P. Fiedler and V. Braun, *Eur. J. Biochem.*, 1979, **99**, 517–524.

38 T. Zheng, J. L. Bullock and E. M. Nolan, *J. Am. Chem. Soc.*, 2012, **134**, 18388–18400.

39 E. K. Dolence, A. A. Minnick, C. E. Lin, M. J. Miller and S. M. Payne, *J. Med. Chem.*, 1991, **34**, 968–978.

40 C. J. Adams, J. J. Wilson and E. Boros, *Mol. Pharm.*, 2017, **14**, 2831–2842.

41 C. J. Adams, J. J. Wilson and E. Boros, *Mol. Pharm.*, 2017, **14**, 2831–2842.

42 R. E. Juárez-Hernández, P. A. Miller and M. J. Miller, *ACS Med. Chem. Lett.*, 2012, **3**, 799–803.

43 E. W. Hunsaker and K. J. Franz, *Inorg. Chem.*, 2019, **58**, 13528–13545.

44 A. Pramanik, U. Stroeher, J. Krejci, A. Standish, E. Bohn, J. Paton, I. Autenrieth and V. Braun, *Int. J. Med. Microbiol.*, 2007, **297**, 459–469.

45 W. Saenger, in *Handbook of Proteolytic Enzymes*, 2013, vol. 3, pp. 3240–3242.

46 S. Konetschny-Rapp, G. Jung, J. Meiwes and H. Zahner, *Eur. J. Biochem.*, 1990, **191**, 65–74.

47 M. van Oosten, T. Schäfer, J. A. C. Gazendam, K. Ohlsen, E. Tsompanidou, M. C. de Goffau, H. J. M. Harmsen, L. M. A. Crane, E. Lim, K. P. Francis, L. Cheung, M. Olive, V. Ntziachristos, J. M. van Dijl and G. M. van Dam, *Nat. Commun.*, 2013, **4**, 2584.

48 T. Hertlein, V. Sturm, U. Lorenz, K. Sumathy, P. Jakob and K. Ohlsen, *Antimicrob. Agents Chemother.*, 2014, **58**, 1630–1638.

49 T. Hertlein, V. Sturm, U. Lorenz, K. Sumathy, P. Jakob and K. Ohlsen, *Antimicrob. Agents Chemother.*, 2014, **58**, 1630–1638.

50 Y. Li, F. Daryaee, G. E. Yoon, D. Noh, P. M. Smith-Jones, Y. Si, S. G. Walker, N. Turkman, L. Meimetis and P. J. Tonge, *ACS Infect. Dis.*, 2020, **6**, 2249–2259.